FISEVIER

Contents lists available at ScienceDirect

# Journal of Magnetism and Magnetic Materials

journal homepage: www.elsevier.com/locate/jmmm



# Strain engineering of magnetic proximity effect and spin-orbit torque in heavy metal/ferromagnet heterostructures



Yuejie Zhang<sup>a,b</sup>, Xiaofei Yang<sup>a</sup>, Peng Li<sup>b,\*</sup>, Mingzhong Wu<sup>b</sup>

- <sup>a</sup> School of Optical and Electronic Information, Huazhong University of Science and Technology, Wuhan, Hubei 430074, China
- <sup>b</sup> Department of Physics, Colorado State University, Fort Collins, CO 80523, USA

#### ABSTRACT

Spin-orbit torque (SOT) has been proposed as an efficient mechanism to switch the magnetization in heavy metal/ferromagnet heterostructures. Several experiments show controversial results on the relationship between the magnetic proximity effect (MPE) and the SOT efficiency in heavy metal/ferromagnet structures. In this work, we use first-principles calculations to investigate the dependence of the MPE and the SOT efficiency on the Pt/CoFe interfacial strain in a model structure of Pt/CoFe/MgO. We have found that the interfacial strain can effectively reduce electron hybridization between Pt and CoFe and thereby significantly suppress the MPE while enhance the SOT efficiency. Thermodynamic magnetics analysis further confirmed these findings. Our results have pointed out a new research direction in which one uses interfacial strain as an effective route to design efficient spintronic devices.

#### 1. Introduction

Spin-transfer-torque magnetic random-access memory (STT-MRAM) is a non-volatile type solid state memory device and has been considered as a promising candidate for future embedded memory applications [1,2]. As STT-MRAM relies on the spin filtering effect, the efficiency of generating a spin torque cannot exceed one. The spin Hall effect has been proposed as an alternate mechanism to realize more efficient magnetization switching at a reduced current. This type of device is generally made of a heavy metal/ferromagnet bi-layered heterostructure. When an electric current flows in the heavy metal, it generates a spin-orbit torque (SOT) which acts on the ferromagnet and switch its magnetization [3-8]. On the other hand, the ferromagnet layer can induce magnetic moments in the neighboring heavy metal layer via the so-called magnetic proximity effect (MPE); it is very intriguing how those induced magnetic moments affect the efficiency of the SOT switching in the heavy metal (HM)/ferromagnet (FM) heterostructure.

There are already several studies devoted to answer this question. Since the MPE strength is inversely proportional to temperature [9,10], One can use temperature dependent measurements to map the relationship between the SOT efficiency and the MPE strength. In a recent work, Zhang et al. demonstrated that the induced magnetic moments were inversely proportional to the spin Hall conductivities in heavy metals Pt and Pd [11]. In a related work, Peterson et al. demonstrated the suppression of the Rashba SOT efficiency as the MPE strength increases in FM/Pt bilayers [12]. These experiments have implied that the

Those experimental findings have motivated us to understand the connection between the spin-orbit torque and the magnetic proximity effect using first-principles calculations. We examined the magnetic moments, density of states, spin polarization, and bonding status of the Pt atoms at the interfaces of Pt/CoFe heterostructures. We also proposed and demonstrated the use of interfacial strain between the heavy metal and the ferromagnet to largely modulate the MPE and thereby significantly enhance the SOT efficiency.

# 2. Method

Our first-principles calculations were performed by using the Vienna ab initio simulation package (VASP) [14–16], with a generalized gradient approximation (GGA) and the projector augmented wave (PAW) potentials [17]. We considered a structure with six Pt monolayers, corresponding to about 1.1 nm, which had been previously identified as the effective spin-polarized Pt layer thickness in experiments [18]. Fig. 1 shows schematically the Ta/MgO/CoFe/Pt/substrate heterostructure that was considered for the simulations. A 15-Å-thick vacuum layer is included on the top. For the calculations, we focused on the MPE at the Pt/CoFe interface. To minimize the lattice mismatch with CoFe, a face-center-cubic structure was used for the 5d metal Pt,

E-mail address: pzl0047@auburn.edu (P. Li).

MPE can affect the SOT efficiency. However, controversial results had been demonstrated in other experiments. For example, it was found that the MPE had no connection with the magnitudes of the damping-like and field-like SOTs after annealing the heterostructures at different conditions [13].

<sup>\*</sup> Corresponding author.

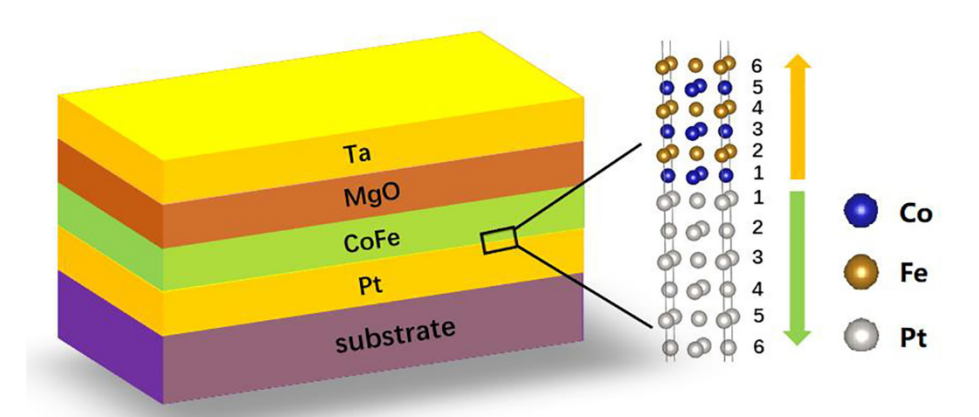


Fig. 1. Schematics of a Ta/MgO/CoFe/Pt/substrate multi-layer structure used in our calculation. The inset on the right shows the atomic structure at the CoFe/Pt interface. The number indicates the atomic layer starting from the Pt/CoFe interface.

with Pt [001] direction [19] being parallel to the CoFe [001] direction [20,21]. The structure was considered fully relaxed until the residual force was less than 0.01 eV/Å. We used a cut-off energy of 540 eV and a K-point mesh of  $20 \times 20 \times 1$ , which ensured good convergences. We used a Pt lattice parameter  $a=3.9239\,\text{Å}$  when the strain is zero [22].

## 3. Results and discussions

Fig. 2 shows our results of the magnetic moment of Pt, Co, and Fe as a function of the layer number. We considered three cases: zero strain  $(a_{Pt} = 3.9239 \,\text{Å})$ , 5% strain  $(a_{Pt} = 3.728 \,\text{Å})$ , and 10% strain  $(a_{Pt} = 3.531 \text{ Å})$ . The magnetic moment per atom  $(\mu)$  is calculated as  $\mu = n(E_{\uparrow}) - n(E_{\downarrow})$ , where  $n(E_{\uparrow})$  and  $n(E_{\downarrow})$  are the number of electrons of different spin states. The unit of  $\mu$  is Bohr magneton ( $\mu_{\rm R}$ ) per atom [23]. According to the X-ray magnetic circular dichroism (XMCD) experiments [24-26], the maximum magnetic moment of Pt in a Co/Pt structure is 0.68  $\mu_{B}/\text{atom}$  [24], and the maximum magnetic moment of Pt in a Fe/Pt structure ranges from  $0.5 \mu_B/atom$  to  $0.62 \mu_B/atom$ [18,19,24]. In our calculations, the maximum magnetic moment  $(\mu)$  of Pt in Pt/CoFe is 0.59  $\mu_{\rm R}$ /atom at zero strain, which has reproduced the experimental values. When the strain increases to 10%, the magnetic moment of Pt atoms in each layer has decreased by over 80%, as shown in Fig. 2(a). However, the magnetic moments ( $\mu$ ) of CoFe in the Pt/ CoFe structure is almost constant at different strain levels, as shown in Fig. 2(b). This indicates that the magnetic moment in Pt does not depend on the magnetization of the neighboring ferromagnet; instead, it is solely sensitive to the interfacial strain. Those calculation results are consistent with the Polarized Neutron Reflectometry (PNR) and X-ray Resonant Magnetic Reflectivity (XRMR) measurements on Pt/CoFeTaB/Pt structures, in which the MPE vanishes whilst the magnetization of the ferromagnet remains [27].

With the theoretical model of the MPE derived in [28], the Hamiltonian can be formulated as:  $H = H_{FM} + H_{HM/FM} + H_{HM}$ , where  $H_{FM}$ ,  $H_{HM}$ , and  $H_{HM/FM}$  are for the ferromagnet, the heavy metal, and their coupling, respectively, which can be written as the following [29]:

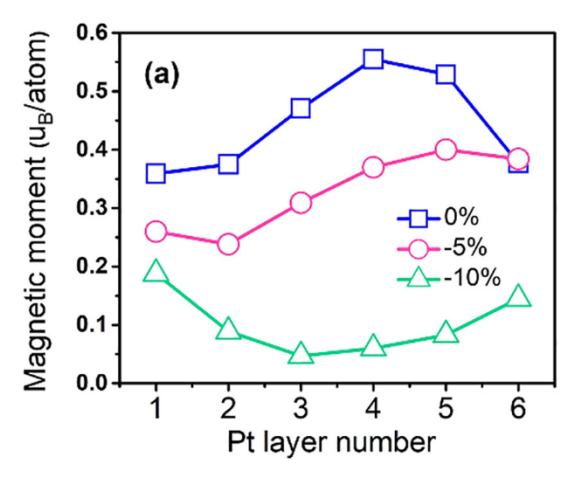
$$H_{FM} = \varepsilon_{FM} \sum_{j,\sigma} c_{j,\sigma}^{\dagger} c_{j,\sigma} + t_{FM} \sum_{\langle i,j \rangle} \sum_{\sigma} \left[ c_{i,\sigma}^{\dagger} c_{j,\sigma} + c_{j,\sigma}^{\dagger} c_{i,\sigma} \right] + U \sum_{i} \sum_{\sigma} \bigcap_{i,\sigma}^{\wedge} n_{i,-\sigma}^{\wedge}$$

$$\tag{1}$$

$$H_{HM} = \varepsilon_{HM} \sum_{j,\sigma} c_{j,\sigma}^{\dagger} c_{j,\sigma} + t_{HM} \sum_{\langle i,j \rangle} \sum_{\sigma} \left[ c_{i,\sigma}^{\dagger} c_{j,\sigma} + c_{j,\sigma}^{\dagger} c_{i,\sigma} \right]$$
 (2)

$$H_{HM/FM} = t_{HM/FM} \sum_{\langle i,j \rangle} \sum_{\sigma} \left[ c_{i,\sigma}^{\dagger} c_{j,\sigma} + c_{j,\sigma}^{\dagger} c_{i,\sigma} \right]$$
(3)

here,  $c_{j,\sigma}^{\dagger}$  and  $c_{j,\sigma}$  are the spin electron creation and destruction operators at lattice site j, respectively.  $\varepsilon_{FM}$  and  $\varepsilon_{HM}$  are the FM and HM band centers, and < i, j > denotes only nearest neighbor summation.  $t_{FM}$ ,  $t_{HM}$  and  $t_{HM/FM}$  are the hopping matrix elements for the FM, the HM, and the HM/FM interface, respectively. U is the Hubbard exchange constant. Eqs. (1)–(3) comprise the creation operators, the destruction operator, and the hopping matrix elements. Those equations allow the characterization of the transfer of the interface charge, so the valence charge density difference (CDD) ( $\rho_{CDD}$ ) distribution can be calculated.



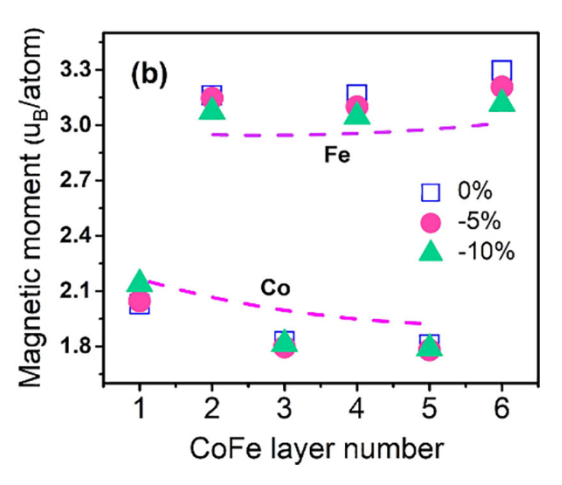


Fig. 2. Effect of strain on the magnetic moment at different layers near the Pt/CoFe interface. (a) Magnetic moment in Pt at different layers. (b) Magnetic moment in the CoFe at different layers.

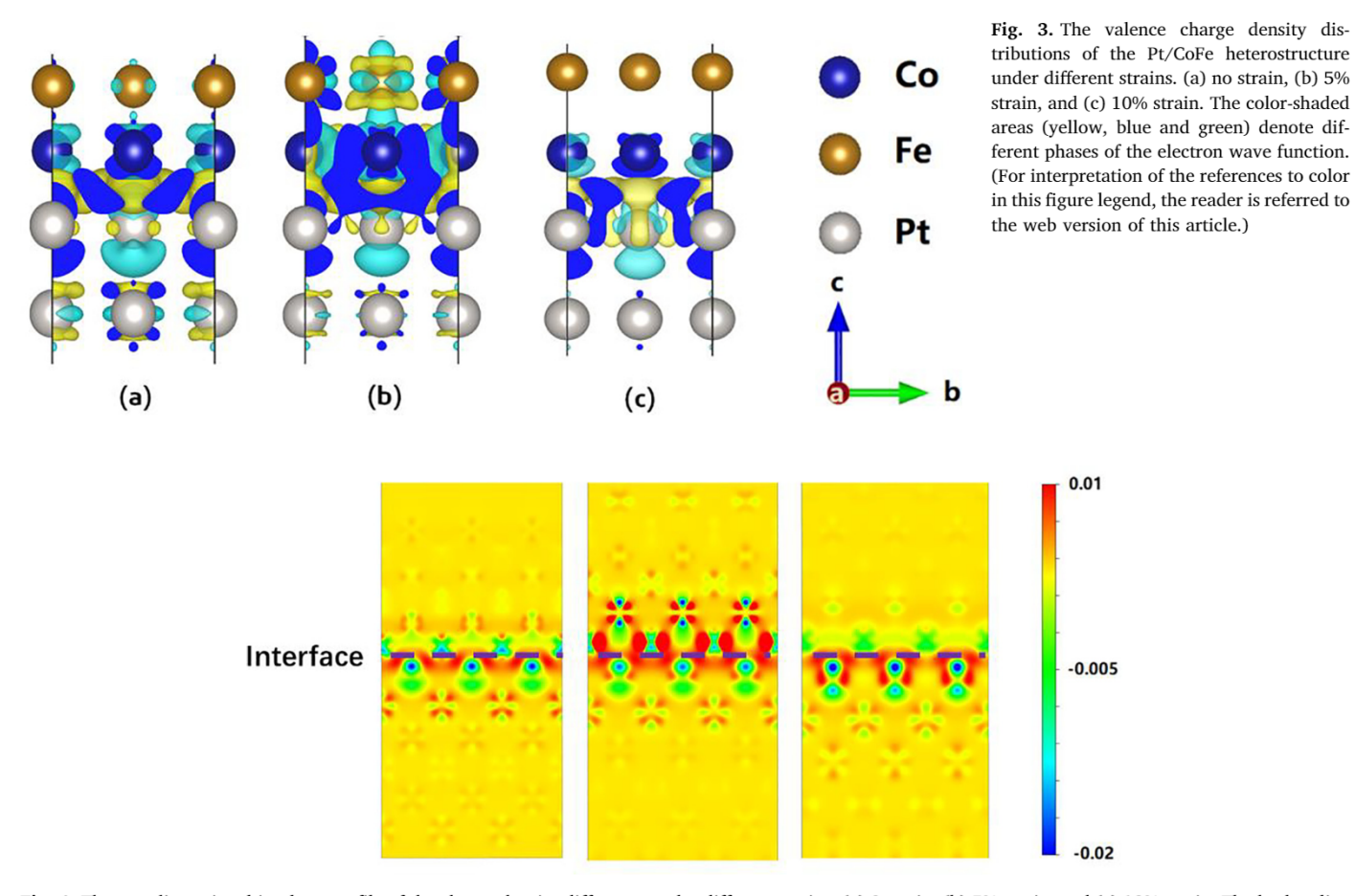


Fig. 4. The two-dimensional in-plane profile of the charge density difference under different strains. (a) 0 strain, (b) 5% strain, and (c) 10% strain. The broken line indicates the Pt/CoFe interface.

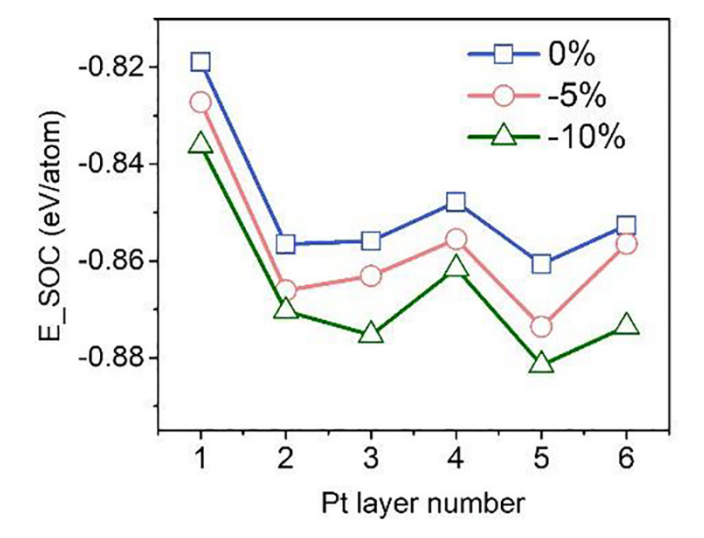


Fig. 5. Dependence of SOC energy on the Pt layer thickness with different interfacial strain levels.

This distribution is defined as  $\rho_{CDD} = \rho_{Pt/CoFe} - \rho_{Pt} - \rho_{CoFe}$  [30], where  $\rho_{Pt/CoFe}$ ,  $\rho_{Pt}$ , and  $\rho_{CoFe}$  denote the charge density distributions of the Pt/CoFe heterostructure, the Pt slab, and the CoFe slab, respectively. The calculation results are presented in Fig. 3, showing a  $\rho_{CDD}$  value of 0.0035. With the increase of the interfacial strain,  $\rho_{CDD}$  in Pt decreases. Note that the charge transfer of the second layer Pt can serve as a reference. The amount of the interfacial charge also decreases significantly, which means that the charge hybridization between the

CoFe layer and the Pt layer decreased with an increase in the interfacial strain.

We calculated the profiles of the two-dimensional in-plane profile of the charge density difference under different strains and present them in Fig. 4. With an increase in the strain, the spacing of the Pt atoms decreases and the electron density of the Pt increases. When the strain is 10%, the majority of the electrons at the interface come from the Pt atoms

Nevertheless, besides the interfacial charge transfer, the spin-orbit coupling (SOC) can also affect the MPE [27,31–33]. In the following, we present our calculations on the SOC energy in Pt and thereby discuss the relationship between the SOC and the MPE.

The spin-orbit term is evaluated by the use of the second-order approximation [34] implemented in VASP:

$$H_{SOC} = \frac{\hbar^2}{4m^2c^2} \frac{1}{r} \frac{\partial V}{\partial r} \vec{L} \cdot \vec{s}$$
 (4)

where L is the angular-momentum operator,  $\overrightarrow{s}$  are the Pauli spin matrices, and V is the spherical part of the all-electron Kohn-Sham potential inside the PAW spheres. Fig. 5 shows the calculation results. With an increase in the strain, the SOC energy increases, which results in the increase of the spin-orbit torque [34–37]. However, the increase in the SOC energy does not reveal whether the increase in the SOC energy is due to the reduction of r or the enhancement of the  $\overrightarrow{L} \cdot \overrightarrow{s}$  matrix; it's unclear whether the SOC  $(\overrightarrow{L} \cdot \overrightarrow{s})$  exists between the Pt atoms or between the Pt and CoFe atoms.

Eq. (3) indicates that the MPE is mainly due to  $t_{HM/FM}$ , exhibiting the importance of the interaction between Pt and CoFe. We calculated the projected density of states (PDOS) between the first Pt layer (Pt<sub>1</sub>)

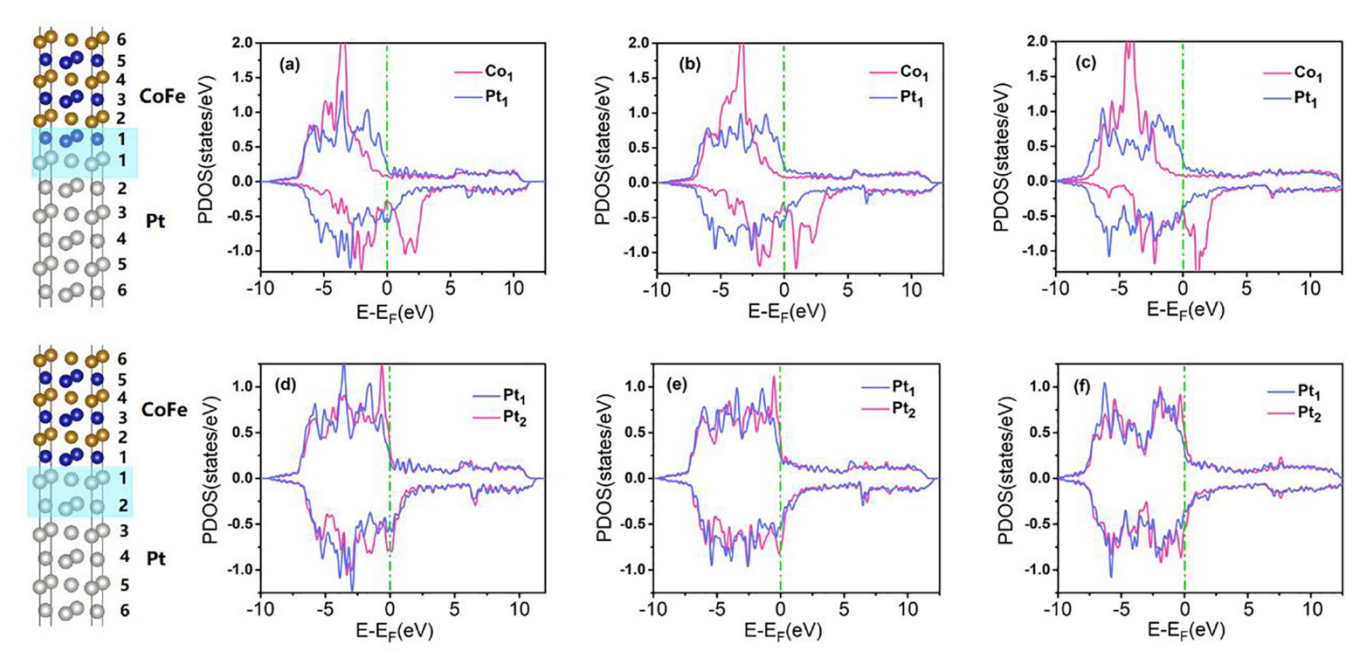


Fig. 6. Projected density of states (PDOS) at different interfaces in Pt/CoFe. Under (a) zero strain, (b) 5% strain, and (c) 10% strain, PDOS between the first Pt layer (Pt<sub>1</sub>) and the first Co layer (Co<sub>1</sub>). Under (d) zero strain, (e) 5% strain, and (f) 10% strain, PDOS between the first Pt layer (Pt<sub>1</sub>) and the second Pt layer (Pt<sub>2</sub>).

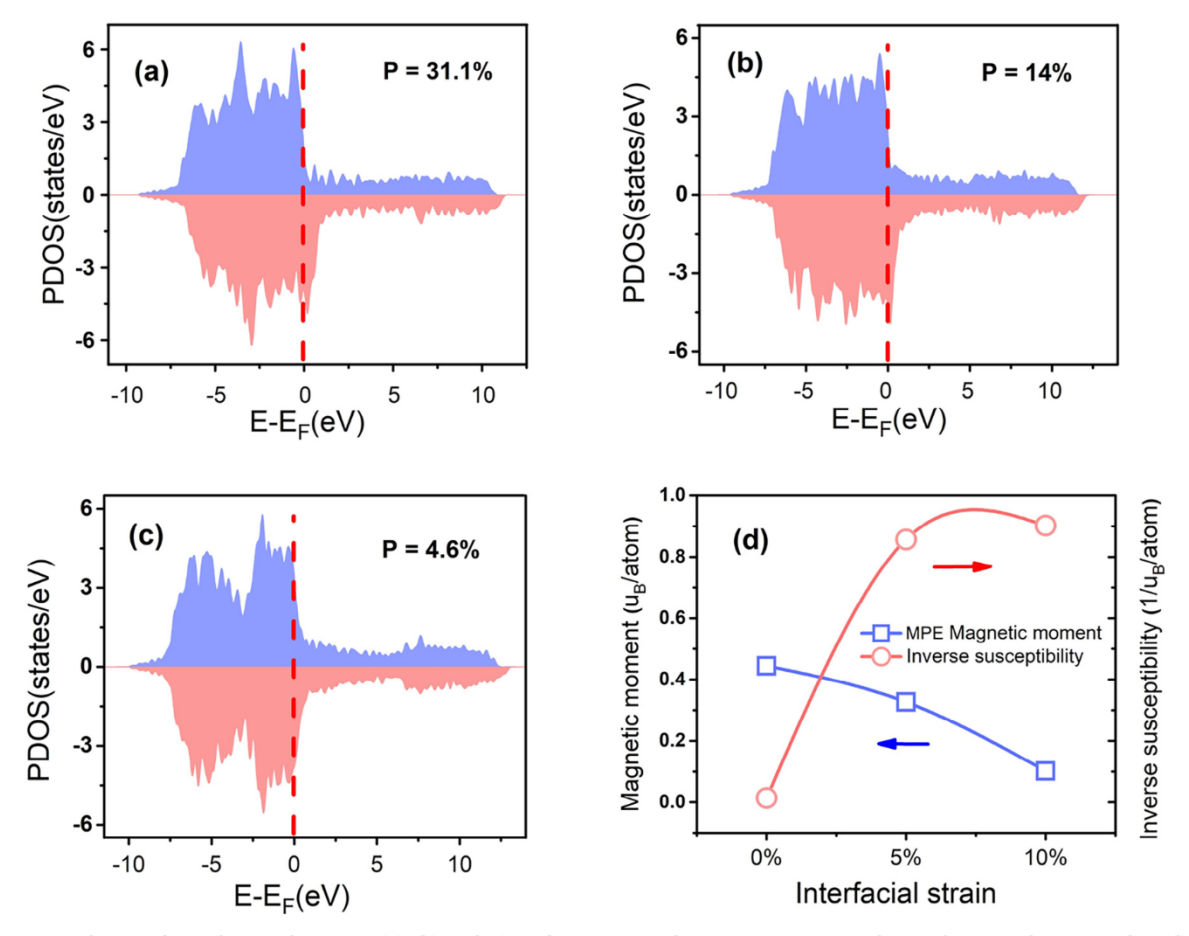


Fig. 7. Electron state density of Pt and spin polarization. (a), (b), and (c) are for 0%, 5%, and 10% strains, respectively. P is the spin polarization of Pt. (d) The inverse susceptibility  $(\alpha)$  and the average magnetic moment  $(\bar{M})$  of Pt as a function of the interfacial strain in Pt/CoFe.

and the first Co layer  $(Co_1)$ , and between the first Pt layer  $(Pt_1)$  and the second Pt layer  $(Pt_2)$ . The results are summarized in Fig. 6. The increase of the interfacial strain promoted the electron hybridization between Pt<sub>1</sub> and Pt<sub>2</sub>, as shown in Fig. 6(d)–(f)); this is in stark contrast to the

case for  $Pt_1$  and  $Co_1$  shown in Fig. 6(a)–(c), in which the electron hybridization weakens with the increase of the interfacial strain. These results have implied that the SOT the Pt layer increases but the MPE is suppressed.

This phenomenon can be understood by referring to the Pauli exclusion principle: when the distance between the Pt atoms decreases, the repulsive force of  $\vec{L} \cdot \vec{s}$  matrix becomes stronger in Pt, and it is difficult for the charge to diffuse from the Co interface into the Pt layer. As a result, the SOC of the Pt layer increases while the MPE response is suppressed.

In the following, we analyzed the MPE using thermodynamic magnetics [10], which describes the problem by the phenomenological free energy density function:

$$f(x,T) = \frac{\alpha(T)}{2}M^2 + \frac{\gamma(T)}{2} \left[\frac{dM}{dx}\right]^2 - M \cdot H$$
 (5)

where M is the local magnetization,  $\gamma(T)$  is the exchange stiffness,  $\alpha(T)$  is the inverse susceptibility. The first term  $\frac{\alpha(T)}{2}M^2$  describes the spin polarizability of Pt, the second term  $\frac{\gamma(T)}{2} \left[\frac{dM}{dx}\right]^2$  describes the spatial spin correlations, and the last term  $M \cdot H$  is the Zeeman energy. Thus, we can calculate the spin polarization, which is defined as a difference between the minority and majority states normalized by the total density of states at the Fermi level, i.e.,  $P = \frac{n_1(E_F) - n_1(E_F)}{n_1(E_F) + n_1(E_F)} \times 100\%$  [30]. The results of projected density of state of Pt are shown in Fig. 7.

The results of projected density of state of Pt are shown in Fig. 7. The spin polarization of Pt is 31.1% (at zero strain), 14% (5% strain), and 4.6% (10% strain). The calculated results show that the spin polarization in Pt decreases with the increase of the interfacial strain, which is consistent with our previous analysis with the quantum theory. Based on the phenomenological free energy density function  $P = \frac{\alpha(T)}{2}M^2$ , we calculated the inverse susceptibility ( $\alpha$ ) and the average magnetic moment (M),  $M = \frac{M_1 + M_2 + \dots + M_6}{6}$ , where  $M_n$  is the local magnetization intensity of the n<sup>th</sup> layer of Pt. The calculated results are shown in Fig. 7(d). The average local magnetic moment (M) decreases while the inverse susceptibility ( $\alpha$ ) increases with the increase of the interfacial strain, which is consistent with our analysis with quantum theory.

## 4. Conclusion

In this work, we used the first-principles calculations to study the effects of interfacial strain on the MPE and the SOT in the Pt/CoFe/MgO structure. We calculated the valence charge density difference (CDD) and the projected density of state (PDOS); our calculations indicate that, with the increase of the strain, the reduction of charge hybridization between Pt and CoFe resulted in weaker MPE responses but stronger SOT. We also calculated the MPE behavior with thermodynamic theory, and we found the same MPE-interfacial strain dependence. This work offers a new route to engineer SOT devices for higher efficiencies.

## **Declaration of Competing Interest**

The authors declare that they have no known competing financial interests or personal relationships that could have appeared to influence the work reported in this paper.

# Acknowledgements

We are grateful for the support of the National Natural Science Foundation of China (No. 11574096); the Graduates' Innovation Fund, Huazhong University of Science and Technology (No. 5003182006); and the U.S. National Science Foundation (No. EFMA-1641989 and No. ECCS-1915849). We are grateful to Professor Ling Miao at Huazhong University of Science and Technology for discussions on the calculations.

#### Appendix A. Supplementary data

Supplementary data to this article can be found online at https://doi.org/10.1016/j.jmmm.2019.166112.

#### References

- [1] H. Kubota, A. Fukushima, K. Yakushiji, T. Nagahama, S. Yuasa, K. Ando, H. Maehara, Y. Nagamine, K. Tsunekawa, D. Djayaprawira, N. Watanabe, Y. Suzuki, Quantitative measurement of voltage dependence of spin-transfer torque in MgObased magnetic tunnel junctions, Nat. Phys. 4 (2008) 37.
- [2] R. Cheng, Q. Niu, Microscopic derivation of spin-transfer torque in ferromagnets, Phys. Rev. B 88 (2013) 024422.
- [3] L. Liu, C.F. Pai, Y. Li, H. Tseng, D. Ralph, R. Buhrman, Spin-torque switching with the giant spin Hall effect of tantalum, Science 336 (2012) 555.
- [4] A. Chernyshov, M. Overby, X. Liu, J.K. Furdyna, Y. Lyanda-Geller, L.P. Rokhinson, Evidence for reversible control of magnetization in a ferromagnetic material by means of spin–orbit magnetic field, Nat. Phys. 5 (2009) 656.
- [5] G. Yu, P. Upadhyaya, Y. Fan, J.G. Alzate, W. Jiang, K.L. Wong, S. Takei, S.A. Bender, L.T. Chang, Y. Jiang, Switching of perpendicular magnetization by spin-orbit torques in the absence of external magnetic fields, Nat. Nanotechnol. 9 (2014) 548.
- [6] A. Brataas, A.D. Kent, H. Ohno, Current-induced torques in magnetic materials, Nat. Mater. 11 (2012) 372.
- [7] P. Li, T. Liu, H. Chang, A. Kalitsov, W. Zhang, G. Csaba, W. Li, D. Richardson, A. DeMann, G. Rimal, H. Dey, J.S. Jiang, W. Porod, S.B. Field, J. Tang, M.C. Marconi, A. Hoffmann, O. Mryasov, M. Wu, Spin-orbit torque-assisted switching in magnetic insulator thin films with perpendicular magnetic anisotropy. Nat. Commun. 7 (2016) 12688.
- [8] D.C. Mahendra, R. Grassi, J. Chen, D. Mahdi Jamali, D Zhang Hickey, Z. Zhao, H. Li, P. Quarterman, Y. Lv, M. Li, A. Manchon, K. Andre Mkhoyan, T. Low, J. Wang, Room-temperature high spin-orbit torque due to quantum confinement in sputtered Bi x Se (1-x) films, Nat. Mater. 17 (2018) 800.
- [9] F. Maccherozzi, M. Sperl, G. Panaccione, J. Minár, S. Polesya, H. Ebert, U. Wurstbauer, M. Hochstrasser, G. Rossi, G. Woltersdorf, Evidence for a magnetic proximity effect up to room temperature at Fe/(Ga, Mn) As interfaces, Phys. Rev. Lett. 101 (2008) 267201.
- [10] W.L. Lim, N. Ebrahim-Zadeh, J. Owens, H.G. Hentschel, S. Urazhdin, Temperature-dependent proximity magnetism in Pt, Appl. Phys. Lett. 102 (2013) 162404.
- [11] W. Zhang, M.B. Jungfleisch, W. Jiang, Y. Liu, J.E. Pearson, S.G. te Velthuis, A. Hoffmann, F. Freimuth, Y. Mokrousov, Reduced spin-Hall effects from magnetic proximity, Phys. Rev. B 91 (2015) 115316.
- [12] T. Peterson, A. McFadden, C. Palmstrøm, P. Crowell, Influence of the magnetic proximity effect on spin-orbit torque efficiencies in ferromagnet/platinum bilayers, Phys. Rev. B 97 (2018) 020403.
- [13] L.J. Zhu, D.C. Ralph, R.A. Buhrman, Irrelevance of magnetic proximity effect to spin-orbit torques in heavy-metal/ferromagnet bilayers, Phys. Rev. B 98 (2018) 134406.
- [14] G. Kresse, J. Hafner, Ab initio molecular dynamics for liquid metals, Phys. Rev. B 47 (1993) 558.
- [15] G. Kresse, J. Furthmuller, Chemisorption of H on Pd(111): an ab initio approach with ultrasoft pseudopotentials, Phys. Rev. B 54 (1996) 11169.
- [16] G. Kresse, J. Furthmuller, Ab initio molecular dynamics for open-shell transition metals, Phys. Rev. B 48 (1993) 13115.
- [17] P.E. Blöchl, Projector augmented-wave method, Phys. Rev. B 50 (1994) 17953.
- [18] C. Klewe, T. Kuschel, J.-M. Schmalhorst, F. Bertram, O. Kuschel, J. Wollschläger, J. Strempfer, M. Meinert, G. Reiss, Static magnetic proximity effect in Pt/Ni<sub>1-x</sub> Fe<sub>x</sub> bilayers investigated by x-ray resonant magnetic reflectivity, Phys. Rev. B 93 (2016) 214440.
- [19] W.J. Antel, Jr., M.M. Schwickert, Tao Lin, W.L. O'Brien, G.R. Harp. Induced ferromagnetism and anisotropy of Pt layers in Fe/Pt (001) multilayers. Phys. Rev. B 2018, 60, 12933.
- [20] S. Peng, W. Zhao, J. Qiao, L. Su, J. Zhou, H. Yang, Q. Zhang, Y. Zhang, C. Grezes, P.K. Amiri, K.L. Wang, Giant interfacial perpendicular magnetic anisotropy in MgO/ CoFe/capping layer structures, Appl. Phys. Lett. 110 (2017) 072403.
- [21] Y. Miura, M. Tsujikawa, M. Shirai, A first-principles study on magnetocrystalline anisotropy at interfaces of Fe with non-magnetic metals, J. Appl. Phys. 113 (2017) 233908.
- [22] H.P. Rooksby, B. Lewis, Relations between the structures of phases in the system platinum-molybdenum, J. Less Common Metals 6 (1964) 451.
- [23] L. Xiao, L. Wang, Structures of platinum clusters: planar or spherical? J. Phys. Chem. A 108 (2004) 8605.
- [24] F. Wilhelm, P. Poulopoulos, A. Scherz, H. Wende, K. Baberschke, M. Angelakeris, N. Flevaris, J. Goulon, A. Rogalev, Interface magnetism in 3d/5d multilayers probed by X-ray magnetic circular dichroism. Phys. Status Solidi (a) 196 (2003) 33.
- [25] F. Wilhelm, P. Poulopoulos, G. Ceballos, H. Wende, K. Baberschke, P. Srivastava, D. Benea, H. Ebert, M. Angelakeris, N. Flevaris, Layer-resolved magnetic moments in Ni/Pt multilayers. Phys. Rev. Lett. 85 (2000) 413.
- [26] T. Kuschel, C. Klewe, J.M. Schmalhorst, F. Bertram, O. Kuschel, T. Schemme, J. Wollschläger, S. Francoual, J. Strempfer, A. Gupta, Static magnetic proximity effect in Pt/NiFe<sub>2</sub>O<sub>4</sub> and Pt/Fe bilayers investigated by X-ray resonant magnetic reflectivity, Phys. Rev. Lett. 115 (2015) 097401.
- [27] O. Inyang, L. Bouchenoire, B. Nicholson, M. Tokac, R.M. Rowan-Robinson, C.J. Kinane, A.T. Hindmarch. Threshold interface magnetization required to induce

- magnetic proximity effect. arXiv preprint arXiv:1902.04308 (2019).
- [28] B. Cox, R. Tahir-Kheli, R. Elliott, Thin films of itinerant-electron ferromagnets on a nonmagnetic metallic substrate, Phys. Rev. B 20 (1979) 2864.
- [29] M. Kiwi, Origin of the magnetic proximity effect, MRS Online Proc. Library Arch. (2002,) 746.
- [30] X. Liang, Y. Zhu, B. Peng, L. Deng, J. Xie, H. Lu, M. Wu, L. Bi, Influence of interface structure on magnetic proximity effect in Pt/Y<sub>3</sub>Fe<sub>5</sub>O<sub>12</sub> heterostructures, ACS Appl. Mater. Interfaces 8 (2016) 8175.
- [31] F. Ma'Mari, T. Moorsom, G. Teobaldi, W. Deacon, T. Prokscha, H. Luetkens, S. Lee, G. Sterbinsky, D. Arena, D. MacLaren, M. Flokstra, M. Ali, M. Wheeler, G. Burnell, B. Hickey, O. Cespedes. Beating the Stoner criterion using molecular interfaces. Nature 2015, 524, 69.
- [32] L. Ma, H. Zhou, L. Wang, X. Fan, W. Fan, D. Xue, K. Xia, Z. Wang, R. Wu, G. Guo,

- L. Sun, X. Wang, X. Cheng, S. Zhou, Spin orbit coupling controlled spin pumping and spin Hall magnetoresistance effects, Adv. Electron. Mater. 2 (2016) 1600112.
- [33] J. Lee, Y. Oh, S. Park, A. Figueroa, G. Laan, G. Go, K. Lee, B. Park, Enhanced spinorbit torque by engineering Pt resistivity in Pt/Co/AlOx structures, Phys. Rev. B 96 (2017) 064405.
- [34] Axel Hoffmann, Spin hall effects in metals, IEEE Trans. Magn. 49 (2013) 5172.
- [35] P. Haney, H. Lee, K. Lee, A. Manchon, M.D. Stiles, Current-induced torques and interfacial spin-orbit coupling, Phys. Rev. B 88 (2013) 214417.
- [36] J. Sklenar, W. Zhang, M.B. Jungfleisch, W. Jiang, H. Saglam, J. Pearson, J. Ketterson, A. Hoffmann, Perspective: interface generation of spin-orbit torques, J. Appl. Phys. 120 (2016) 180901.
- [37] Y. Wang, R. Ramaswamy, H. Yang, FMR-related phenomena in spintronic devices, J. Phys. D Appl. Phys. 51 (2018) 273002.